Nacre morphology and chemical composition in Atlantic winged oyster *Pteria colymbus* (Röding, 1798)

Pablo Santana [1], **Dalila Aldana Aranda** [Corresp. 1]

[1] Departamento de Recursos del Mar, Centro de Investigación y de Estudios Avanzados del Instituto Politécnico Nacional, MERIDA, Yucatán, México

Corresponding Author: Dalila Aldana Aranda
Email address: daldana@cinvestav.mx

The microstructure and nanostructure of nacre in *Pteria colymbus* were studied with high-resolution field emission scanning electron microscopy (FESEM). The tablets were found to be flat and polyhedral with four to eight sides, and lengths ranging from 0.6 to 3.0 µm. They consisted of nanocrystals 41 nm wide, growing in the same direction. X-ray diffraction showed the crystals to be mineral phase aragonite, which was confirmed by Raman spectroscopy. Fourier transform infrared spectroscopy identified a band at 1786.95 cm^{-1} attributed to carboxylate (carbonyl) groups of the proteins present in the organic matrix as well as bands characteristic of calcium carbonate. X-ray fluorescence showed the nacre to contain 98% calcium carbonate, as well as minor elements (Si, Na, S and Sr) and trace elements (Mg, P, Cu, Al, Fe, Cl, K and Zn).

Nacre morphology and chemical composition in Atlantic winged oyster *Pteria colymbus* (Röding, 1798)

Pablo Santana-Flores[1], Dalila Aldana Aranda[1]

[1]Departamento de Recursos del Mar, Centro de Investigación y de Estudios Avanzados, Mérida, Yucatán, México

Corresponding Author:
Dalila Aldana Aranda[1]
Laboratorio de Biología y Acuacultura de Moluscos, Km 6 antigua Carretera a Progreso S/N Cordemex, Mérida, Yucatán, 97310, México
Email address: daldana@cinvestav.mx

Abstract

The microstructure and nanostructure of nacre in Pteria colymbus were studied with high resolution field emission scanning electron microscopy (FESEM). The tablets were found to be flat and polyhedral with four to eight sides, and lengths ranging from 0.6 to 3.0 μm. They consisted of nanocrystals 41 nm wide, growing in the same direction. X-ray diffraction showed the crystals to be mineral phase aragonite, which was confirmed by Raman spectroscopy. Fourier transform infrared spectroscopy identified a band at 1786.95 cm-1 attributed to carboxylate (carbonyl) groups of the proteins present in the organic matrix as well as bands characteristic of calcium carbonate. X-ray fluorescence showed the nacre to contain 98% calcium carbonate, as well as minor elements (Si, Na, S and Sr) and trace elements (Mg, P, Cu, Al, Fe, Cl, K and Zn).

Introduction

Mollusk shells are mineralized tissues that fulfill structural functions (Addadi et al. 2003). In all three main mollusk classes (Cephalopoda, Gastropoda and Bivalvia) the shell consists of stratified layers, each with a unique mineral composition (Dauphin & Denis, 2000). Shell-forming crystals are organized on these layers according to different configurations which define a shell's microstructures. Specific microstructures are characteristic of calcite (i.e., prismatic, foliate) and aragonite (i.e., nacre, laminar cross). Secreted polymorph type and microstructural types are used to characterize large mollusk groups, particularly the bivalves.

Nacre is the most studied aragonitic microstructure and is widely distributed in mollusks (Towe & Hamilton, 1967). Its stratified microstructure gives mother-of-pearl its luster and provides excellent mechanical properties. Nacre has been of great interest to the pearl industry, making it one of the most studied hard tissues (Wang et al., 2013). Because it is osteoconductive and biodegradable, interest has increased recently in technological applications related to nacre, such as the manufacture of bio-inspired super-resistant materials and clinical implants (Oaki and Imai, 2005, Tang et al., 2003).

In each of the three main mollusk classes (Gastropoda, Cephalopoda and Bivalvia) nacre exhibits specific growth patterns and mechanisms. In Gastropoda, for example, the aragonite nanocrystals in the nacre are stacked in towers and their c axes are aligned. However, they have a composite cross laminar arrangement, and a third hierarchical order of flat aragonite fibers from 50 to 100 nm thick, 300 nm wide and a few micrometers long (Romana et al., 2013). In the nautilus (Cephalopoda), nacre exhibits a mixed behavior with simultaneous growth in towers and terraces occurring in adjacent locations (Saunders & Landman, 2010). Nacre in the Bivalvia has terraced growth and the three axes of crystals are co-oriented. The order Pterioidae has shells that are unequal, monomyary, and not equilateral; the right valve is generally less convex than the left (Cummings & Graf, 2015; Wada & Tëmkin, 2008). Their shells are formed by superposition of an outer organic layer, the periostracum, a prismatic layer and the inner nacreous layer (Kennedy et al., 1969).

Nacre is a biomineral consisting (by weight) of 95% aragonite ($CaCO_3$) with the remaining 1 to 5% being organic matrix (Gangsheng Zhang & Li, 2012). Its microstructure is one of layered “brick” (aragonite tablets) and “mortar” (protein-polysaccharide matrix). This structure provides nacre with twice the strength and up to 1000 times the toughness of its constituent components alone (Li et al., 2004; Morris et al., 2016; Veis & Dorvee, 2013). Individual nacre tablets have a nanoscale structure based on aragonite nanograins, nanoblocks and nanofibers (Wang et al., 2013). Nanoscale structural organization differs between bivalve mollusks, resulting in different tablet forms at growth completion.

Better understanding of the composition and hierarchy of biological system microstructures is key in the search for new materials and provides deeper insight into evolutionary processes (Jáuregui-Zúñiga et al., 2003; Nakamura Filho et al., 2014; Oaki & Imai, 2005; Wang et al., 2013; Wegst et al., 2015). The present study objective was to analyze the micro- and nanostructure of *P. colymbus*

nacre with scanning electron microscopy, and its chemical composition with x-ray diffraction, X-ray fluorescence spectrometry, Fourier transform infrared spectrometry and Raman spectroscopy.

Materials & Methods

Shells of *Pteria colymbus* were collected in the Alacranes Reef, in the state of Yucatán, Mexico. They were placed in a soap solution, cleaned, and stored at 4 °C for 48 hours. To remove the inorganic and biogenic matter from shells was cleaned by ultrasound with a soap solution for five minutes. (Ky et al. 2013). Six 1 cm^2 samples were cut from the shells using a 32 mm-diameter diamond disc. Samples were washed again by ultrasound for five minutes and dried at 65 °C for three hours (Ren et al., 2009; Xu & Zhang, 2017).

Nacre tablet morphology was characterized with a JEOL 7600F ultra high resolution field emission scanning electron microscope (FESEM). Samples were coated with Au/Pd and processed at a 1-30 kV acceleration voltage (Liu & Li, 2015; Ren et al., 2009).

Chemical analyses of the shells were done with X-ray diffraction (XRD) (Bruker D8) using monochromatic CuKa radiation. The XRD patterns were collected at 20 to 90 ° (2Θ) in 0.02 ° steps with a 0.96 s count time interval. The resulting diffraction patterns were compared with the cards for calcite (no. 83-578) and aragonite (no. 76-606) from the crystallographic records of the International Center for Diffraction Data (ICDD) database (de Paula & Silveira, 2009; Heinemann et al., 2011; Weiner & Traub, 1980).

Fourier transform infrared spectrometry (FTIR) was done by first pressing nacre powder into KBr tablets (0.5 mg sample/200 mg KBr). Infrared analyzes were run at a 4 cm resolution in two wave ranges: 400-4000 cm^{-1} and 550-4000 cm^{-1}. The analyzes were done in reflectance mode on a FTIR spectrometer with Bruker accessory (EQUINOX 5). Spectra were automatically corrected for water, carbon dioxide and the KBr background (Cardoso et al., 2016; Monarumit et al., 2015; G. Zhang et al., 2016).

Chemical analyses were also done using the semi-quantitative method of X-ray fluorescence spectrometry (XFR) with wave dispersion in a spectrometer (Briker S4 Pioneer) with a 4kW excitation source. A vacuum scan was done of 71 elements (11Na-92U) using an RX tube with Rh anode, 25 to 60 kV excitation voltage, and a 0.46 dg collimator with a 34 mm mask. Data was interpreted with the Spectra Plus software. Quantification of $CaCO_3$ was done with an ignition loss analysis at 950 °C for one hour (Shi et al., 2018).

The $CaCO_3$ crystalline phase was identified using a Raman spectrometer with focal point (WITEC Alpha 300) (λexc = 488 and 785 nm; acquisition time 10 s; resolution 10 cm^{-1}).

Results

Microstructure and nanostructure

The shell of *P. colymbus* consists of a prismatic and an aragonitic layer clearly divided by a slight change in color (Figure 1, indicated by arrow and BL symbol). The FESEM analysis identified an organic hydrogel on some tablets in different layers (Figure 2a). In another growth section of the pearlescent layer small growing crystals were observed to be fusing with each other (Fig. 2b). The tablets form a uniform sheet at the point where the next layer begins to grow and in some cases the tablets fuse with higher layers (Figure 2c). Mature tablets are four to eight-sided, 0.6 to 3.0 µm in length, and can be fused (Figure 2d).

Cross sections of the nacre tablets showed a nanostructure in which the first layer of deposited nacre consisted of packed nanocrystals forming tablets. These were longer than in the upper layers and their growth was perpendicular to the surface (Figure 3a). Crystals in initial growth stages were observed in a section close to the prismatic layer (Figure 3b). In the intermediate section of the shell all the deposited nacre layers contained tablets composed of a package of crystals fused in the “brick and mortar” arrangement typical of species in the Pteriidae family. Average tablet thickness was 385 nm (SD = 0.069) (n = 187) with a range of 200 to 530 nm (Figure 3c). The nanocrystals were uniformly oriented perpendicular to shell surface, have a 41 nm (SD = 9.43) (n = 24) average width, and a length range of 24 to 69 nm (n = 24) (Figure 3d).

Chemical analysis

The XRD pattern of the nacre layer showed the main reflection to be at 31 (2Θ) with two lesser readings at 33.0 (2Θ) and 66.0 (2Θ), both characteristic of aragonite (Figure 4).

The XRF analysis identified aragonite as representing 98.13% of sample weight. Minor elements were Si (0.72%), Na (0.5500%), S (0.2080%), and Sr (0.1042%), and trace elements were Mg (0.0897%), P (0.0485%), Cu (0.0353%), Al (0.0331), Fe (0.0311%), Cl (0.0290%), K (0.0151% and Zn (0.0060%). The nacre’s aragonite structure was confirmed in the FTIR analysis (Figure 5). Four bands characteristic of aragonite, corresponding to the CO_3^{2-} ions, were identified: v3 at 1445.96 cm^{-1}; v1 at 1082.72 cm^{-1}; v2 at 856.80 cm^{-1}; and v4 at 699.81-712.52 cm^{-1}. The v4 band corresponds to the planar flexion mode of carbonate vibration and the v1 band to the symmetric

stretch mode. The nacre FTIR spectrum revealed lower intensity organic bands; the band at 1786.95 cm^{-1} was attributed to the carboxylate (carbonyl) groups of the acidic proteins in the organic matrix.

The Raman spectroscopy analysis of the nacre surface produced the most intense band at near 1085 cm^{-1} in the aragonite spectra which corresponds to symmetrical stretching mode v1 of the carbonate ion (Figure 6). Low- to medium-intensity bands in the 100-300 cm^{-1} region of the aragonite spectra were due to the translational and rotational modes of lattice vibration. The v4 in the carbonate ion plane bending mode occurred as a doublet with bands between 701 and 705 cm^{-1}.

Discussion

Nacre in *P. colymbus* consists of polygonal tablets with four to eight sides, a morphological characteristic also present in species such as *Pinctada maxima*, *Pinctada radiata* and *Pinctada fucata* (Whang et al. 2001, Bellaaj-Zouari et al. 2011, Zhang et al. 2019). However, tablet length differs between species in the Pteriidae family. In *P. colymbus*, length ranges from 0.6 to 3.0 µm, whereas in *P. radiata* it ranges from 4.0 to 5.0 µm (Bellaaj-Zouari et al. 2011), and in *P. margaritifera* from 5.0 to 10.0 µm (Rousseau et al. 2009).

Morphological differences in pearl oysters can be seasonal or intrinsic to each species (Wada 1972). Intrinsic differences are due to genetic control of shell mineralogy and any similarities between species can be traced to the Mesozoic/Paleozoic boundary (Kennedy et al. 1969). Environmental factors such as temperature can modify shell structure in different organisms. For instance, shell aragonite percentage in the mussel *Mytilus californianus* decreases from 45% in the spring to 30% in the winter, but only in organisms longer than 15 mm (Kennedy et al. 1969). Slower nacre deposition rates may be in response to reductions in water temperature, probably in winter, combined with lower food availability (Taylor and Strack 2008). In another example, in *P. fucata* nacre growth and thickness respond to tablet thickness which is 324 nm when water temperature is highest, during August, but only 224 nm when it is lower, in December (Muhammad et al. 2017). Decreases in tablet thickness favor light iridescence of the nacre surface which is why pearl producers harvest pearls when sea water temperature decreases (Nagai 2013).

The tablets in *P. colymbus* shell contain nanocrystals ranging in thickness from 24 to 69 nm. This coincides with tablets in *P. maxima* which consist of aragonite nanofibrils from 10 to 30 nm thick (Wang et al. 2012). Tablets in abalone *Haliotis rufescens* shell are built of parallel aragonite

nanoparticles (Huang and Li 2012), and its nanostructure is one of polygonal cobble-like grains (~32 nm) within individual aragonite tablets (Li et al. 2004). The shell of *P. fucata* contains nanoblocks from 20 to 180 nm long (Oaki and Imai 2005).

In each species formation of the aragonite nanoparticles in nacre tablets is regulated by organic matrix characteristics (Dauphin and Denis, 2000, Kim et al. 2006). The distribution of organic macromolecules during crystal growth is important since these regulate crystal size, shape and orientation (Okumura et al. 2012, Shtukenberg et al. 2017).

Calcium carbonate ($CaCO_3$) in the form of aragonite represents 98.13% of the total nacre layer in *P. colymbus* in the present results. The majority presence of aragonite in the shell coincides with other species in the Pteriidae family, such as *P. fucata* (Saruwatari et al. 2009) and *P. margaritifera* (Shi et al. 2018), as well as the mussel *Perna viridis* (Xu and Zhang 2015). Minor elements are Si, Na, S and Sr, and trace elements are Mg, P, Cu, Al, Fe, Cl, K and Zn. Taylor and Strack (2008) found that nacre is composed of calcium carbonate (91.50%) with traces of organic substances (3.83%), residual substances (0.01%) and water (3.97%). These residual substances include Na, Cl and K, as well as traces and other elements such as Ba, Mg, P, Mn, Fe, Al, Cu, Zn, Ag, Hg, Li and Mr. The trace element profile of a nacre reflects water mineral composition in the place where it formed.

In biogenic aragonite crystals other elements such as Mn, Mg, Sr and Ba can substitute for calcium (Chen et al., 2011; Gaetani & Cohen, 2006). Notable differences in the concentration of these elements exist between taxonomic groups, highlighting genetic influence on their incorporation (Carré et al., 2006).

The other elements present in nacre function as precursor ions in nacre formation, as catalysts in proteins and activators of enzymes; they are present in intercrystalline organic macromolecules and the organism's epithelial fluid (Cho & Jeong, 2011; Marin, 2012; Marsh & Sass, 1983).

Conclusions

Nacre composition in *P. colymbus* has high aragonite content and its nanostructure consists of polygonal tablets built of nanocrystals. The present is a preliminary description of *P. colymbus* carapace structure intended as a presentation of the relevant data to date, and a guide for further research.

Acknowledgements

The authors thank Patricia Quintana access to LANNBIO facilities, Dora Huerta, and Daniel Aguilar for assistance with the diffractograms and SEM images. The authors also thank Maria del Socorro Garcia Guillermo, Ixchel Rubí Perez, Ana Elena Muñiz, and Norma Alicia Berlanga, at Cinvestav-Saltillo chemical analysis General Laboratory for her support in carrying out this work.

References

Cardoso, S. S. S., Cartwright, J. H. E., Checa, A. G., & Sainz-Díaz, C. I. (2016). Fluid-flow-templated self-assembly of calcium carbonate tubes in the laboratory and in biomineralization: The tubules of the watering-pot shells, Clavagelloidea. *Acta Biomaterialia*, *43*(Supplement C), 338-347. https://doi.org/10.1016/j.actbio.2016.07.005

Carré, M., Bentaleb, I., Bruguier, O., Ordinola, E., Barrett, N. T., & Fontugne, M. (2006). Calcification rate influence on trace element concentrations in aragonitic bivalve shells: Evidences and mechanisms. *Geochimica et Cosmochimica Acta*, *70*(19), 4906-4920. https://doi.org/10.1016/j.gca.2006.07.019

Chen, T., Yu, K., Li, S., Chen, T., & Shi, Q. (2011). Anomalous Ba/Ca signals associated with low temperature stresses in Porites corals from Daya Bay, northern South China Sea. *Journal of Environmental Sciences*, *23*(9), 1452-1459. https://doi.org/10.1016/S1001-0742(10)60606-7

Cho, S.-M., & Jeong, W.-G. (2011). Prismatic shell repairs by hemoctyes in the extrapallial fluid of the Pacific Oyster, Crassostrea gigas. *The Korean Journal of Malacology*, *27*(3), 223-228. https://doi.org/10.9710/kjm.2011.27.3.223

Cummings, K. S., & Graf, D. L. (2015). Class Bivalvia1. In *Thorp and Covich's Freshwater Invertebrates* (pp. 423-506). Elsevier. https://doi.org/10.1016/B978-0-12-385026-3.00019-X

Dauphin, Y., & Denis, A. (2000). Structure and composition of the aragonitic crossed lamellar layers in six species of Bivalvia and Gastropoda. *Comparative Biochemistry and Physiology Part A: Molecular & Integrative Physiology*, *126*(3), 367-377. https://doi.org/10.1016/S1095-6433(00)00213-0

de Paula, S. M., & Silveira, M. (2009). Studies on molluscan shells: Contributions from microscopic and analytical methods. *Micron*, *40*(7), 669-690. https://doi.org/10.1016/j.micron.2009.05.006

Gaetani, G. A., & Cohen, A. L. (2006). Element partitioning during precipitation of aragonite from seawater: A framework for understanding paleoproxies. *Geochimica et Cosmochimica Acta*, *70*(18), 4617-4634. https://doi.org/10.1016/j.gca.2006.07.008

Heinemann, F., Launspach, M., Gries, K., & Fritz, M. (2011). Gastropod nacre: Structure, properties and growth — Biological, chemical and physical basics. *Biophysical Chemistry*, *153*(2), 126-153. https://doi.org/10.1016/j.bpc.2010.11.003

Jáuregui-Zúñiga, D., Reyes-Grajeda, J., Sepúlveda-Sánchez, J., Whitaker, JohnR., & Moreno, A. (2003). Crystallochemical characterization of calcium oxalate crystals isolated from seed coats of

Phaseolus vulgaris and leaves of Vitis vinifera. *Journal of Plant Physiology*, *160*(3), 239-245. https://doi.org/10.1078/0176-1617-00947

Kennedy, W. J., Taylor, J. D., & Hall, A. (1969). Environmental and biological controls on bivalve shell mineralogy. *Biological Reviews*, *44*(4), 499-530. https://doi.org/10.1111/j.1469-185X.1969.tb00610.x

Li, X., Chang, W.-C., Chao, Y. J., Wang, R., & Chang, M. (2004). Nanoscale Structural and Mechanical Characterization of a Natural Nanocomposite Material: The Shell of Red Abalone. *Nano Letters*, *4*(4), 613-617. https://doi.org/10.1021/nl049962k

Liu, X., & Li, J. (2015). Formation of the prismatic layer in the freshwater bivalve Hyriopsis cumingii: The feedback of crystal growth on organic matrix. *Acta Zoologica*, *96*(1), 30-36. https://doi.org/10.1111/azo.12048

Marin, F. (2012). The formation and mineralization of mollusk shell. *Frontiers in Bioscience*, *S4*(3), 1099-1125. https://doi.org/10.2741/s321

Marsh, M. E., & Sass, R. L. (1983). Calcium-binding phosphoprotein particles in the extrapallial fluid and innermost shell lamella of clams. *Journal of Experimental Zoology*, *226*(2), 193-203. Scopus. https://doi.org/10.1002/jez.1402260204

Monarumit, N., Noirawee, N., Phlayrahan, A., Promdee, K., Won-in, K., & Satitkune, S. (2015). Identification of High-Luster and Lusterless Freshwater-Cultured Pearls by X-Ray Absorption Spectroscopy. *Journal of Applied Spectroscopy*, *82*(4), 677-680. https://doi.org/10.1007/s10812-015-0163-3

Morris, J. P., Wang, Y., Backeljau, T., & Chapelle, G. (2016). Biomimetic and bio-inspired uses of mollusc shells. *Marine Genomics*, *27*, 85-90. https://doi.org/10.1016/j.margen.2016.04.001

Nakamura Filho, A., Almeida, A. C. de, Riera, H. E., Araújo, J. L. F. de, Gouveia, V. J. P., Carvalho, M. D. de, & Cardoso, A. V. (2014). Polymorphism of $CaCO_3$ and microstructure of the shell of a Brazilian invasive mollusc (Limnoperna fortunei). *Materials Research*, *17*(suppl 1), 15-22. https://doi.org/10.1590/S1516-14392014005000044

Oaki, Y., & Imai, H. (2005). The Hierarchical Architecture of Nacre and Its Mimetic Material. *Angewandte Chemie International Edition*, *44*(40), 6571-6575. https://doi.org/10.1002/anie.200500338

Ren, F., Wan, X., Ma, Z., & Su, J. (2009). Study on microstructure and thermodynamics of nacre in mussel shell. *Materials Chemistry and Physics*, *114*(1), 367-370. https://doi.org/10.1016/j.matchemphys.2008.09.036

Romana, L., Thomas, P., Bilas, P., Mansot, J. L., Merrifiels, M., Bercion, Y., & Aranda, D. A. (2013). Use of nanoindentation technique for a better understanding of the fracture toughness of Strombus gigas conch shell. *Materials Characterization*, *76*, 55-68. Scopus. https://doi.org/10.1016/j.matchar.2012.11.010

Saunders, W. B., & Landman, N. H. (Eds.). (2010). *Nautilus: The Biology and Paleobiology of a Living Fossil, Reprint with additions* (Vol. 6). Springer Netherlands. https://doi.org/10.1007/978-90-481-3299-7

Shi, L., Wang, Y., Liu, X., & Mao, J. (2018). Component analysis and identification of black Tahitian cultured pearls from the oyster Pinctada margaritifera using spectroscopic techniques. *Journal of Applied Spectroscopy*, *85*(1), 98-102. https://doi.org/10.1007/s10812-018-0618-4

Taylor, J. D., & Reid, D. G. (1990). Shell microstructure and mineralogy of the Littorinidae: Ecological and evolutionary significance. *Hydrobiologia*, *193*(1), 199-215. https://doi.org/10.1007/BF00028077

Taylor, J., & Strack, E. (2008). Pearl production. *The Pearl Oyster*, Southgate, P. and Lucas, J., eds. Elsevier: 273-302.

Towe, K. M., & Hamilton, G. H. (1967). Ultrastructure and inferred calcification of the mature and developing nacre in bivalve mollusks. *Calcified Tissue Research*, *1*(1), 306-318. https://doi.org/10.1007/BF02008102

Veis, A., & Dorvee, J. R. (2013). Biomineralization Mechanisms: A new paradigm for crystal nucleation in organic matricies. *Calcified Tissue International*, *93*(4), 307-315. https://doi.org/10.1007/s00223-012-9678-2

Wada, K. T., & Tëmkin, I. (2008). Chapter 2—Taxonomy and Phylogeny. In P. C. Southgate & J. S. Lucas (Eds.), *The Pearl Oyster* (pp. 37-75). Elsevier. https://doi.org/10.1016/B978-0-444-52976-3.00002-4

Wang, S.-N., Yan, X.-H., Wang, R., Yu, D.-H., & Wang, X.-X. (2013). A microstructural study of individual nacre tablet of Pinctada maxima. *Journal of Structural Biology*, *183*(3), 404-411. https://doi.org/10.1016/j.jsb.2013.07.013

Wegst, U. G. K., Bai, H., Saiz, E., Tomsia, A. P., & Ritchie, R. O. (2015). Bioinspired structural materials. *Nature Materials*, *14*(1), 23-36. https://doi.org/10.1038/nmat4089

Weiner, S., & Traub, W. (1980). X-ray diffraction study of the insoluble organic matrix of mollusk shells. *FEBS Letters*, *111*(2), 311-316. https://doi.org/10.1016/0014-5793(80)80817-9

Xu, J., & Zhang, G. (2017). Direct observation of the crystallographic relationship between interlamellar membranes and aragonite tablets in bivalve nacre. *Journal of Structural Biology*, *197*(3), 308-311. https://doi.org/10.1016/j.jsb.2016.12.009

Zhang, G., Willemin, A. S., Brion, A., Piet, M. H., Moby, V., Bianchi, A., Mainard, D., Galois, L., Gillet, P., & Rousseau, M. (2016). A new method for the separation and purification of the osteogenic compounds of nacre ethanol soluble matrix. *Journal of Structural Biology*, *196*(2), 127-137. https://doi.org/10.1016/j.jsb.2016.03.016

Zhang, Gangsheng, & Li, X. (2012). Uncovering aragonite nanoparticle self-assembly in nacre—A natural armor. *Crystal Growth & Design*, *12*(9), 4306-4310. https://doi.org/10.1021/cg3010344

Figure 1

SEM image of *Pteria colymbus* (Mollusca, Bivalvia) shell cross section.

NL: Nacreous layer IL: intermediate layer of shell aragonite layer. BL: Dividing zone between prismatic and aragonite layers. PL: Prismatic layer.

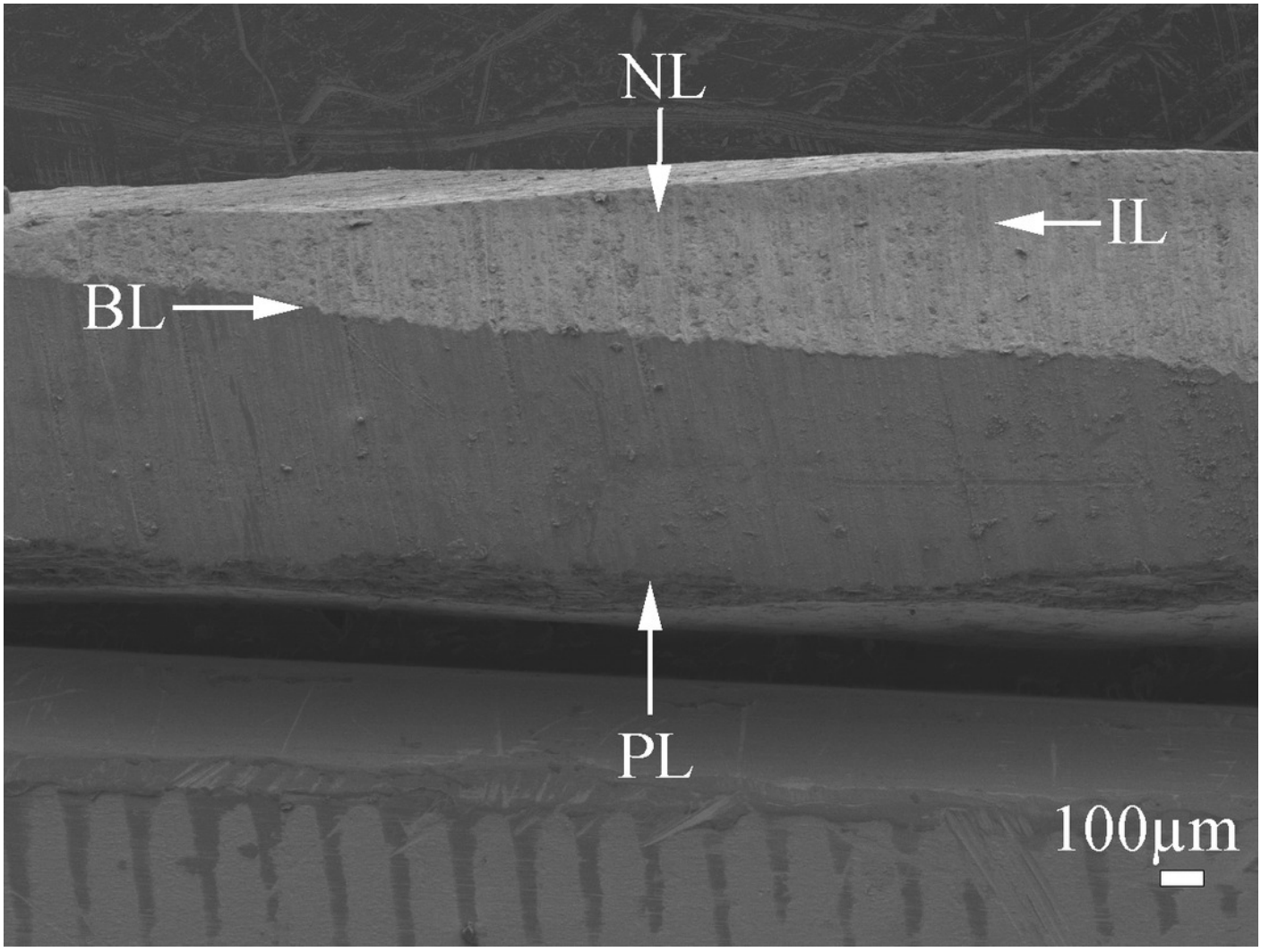

Figure 2

SEM images of internal surface of *Pteria colymbus* (Mollusca, Bivalvia) shell at different scales.

a) Growing nacre tablets with presence of organic hydrogel (indicated by arrows). (b) crystals in different stages of growth (indicated by arrows). Crystal in the first stage of formation (★), crystal fusing with other surrounding crystals (✺). (c) Fused tablets with overlapping layers (indicated by arrow). (d) tablet with minimal polyhedral shape (★) and fused tablet (✺).

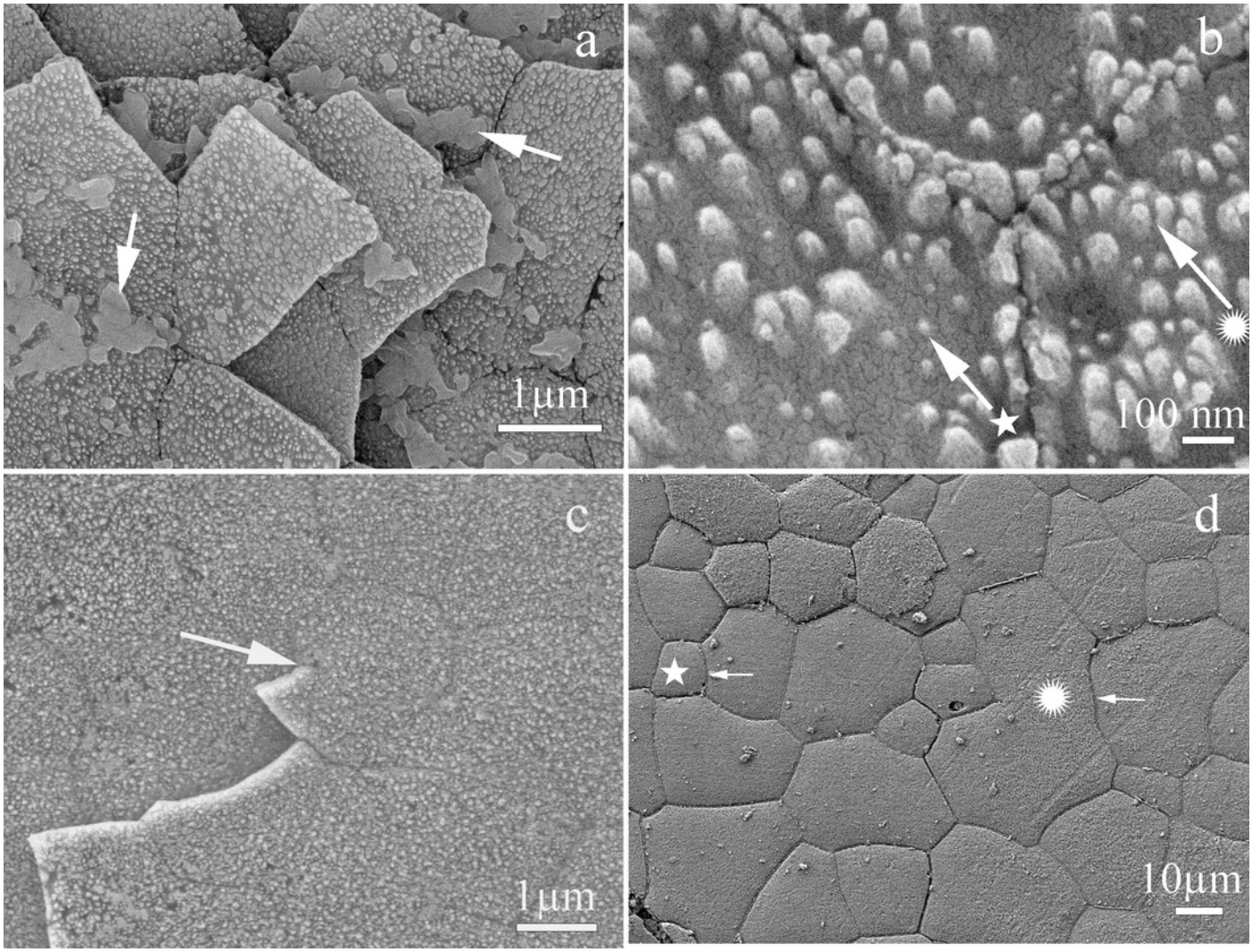

Figure 3

SEM image of *Pteria colymbus* (Mollusca, Bivalvia) shell transversal cross section.

(a) First layer of mother-of-pearl on prismatic structure. Crystals sharing the same growth orientation, perpendicular to the surface (indicated by the arrow). nacre layer with uniform formation (NL). Prismatic layer (PL). (b) Layer of growing crystals over organic hydrogel (H) covering the prismatic layer (PL). Recently formed nacreous crystals (NL). (c) Middle zone of shell nacre layer. Tablets are in “brick and mortar” arrangement (represented by lines). (d) Tablets containing nanocrystals. Regular crystal shapes indicate individual crystal formation (★). Fusion occurred from the center of the crystal (✺).

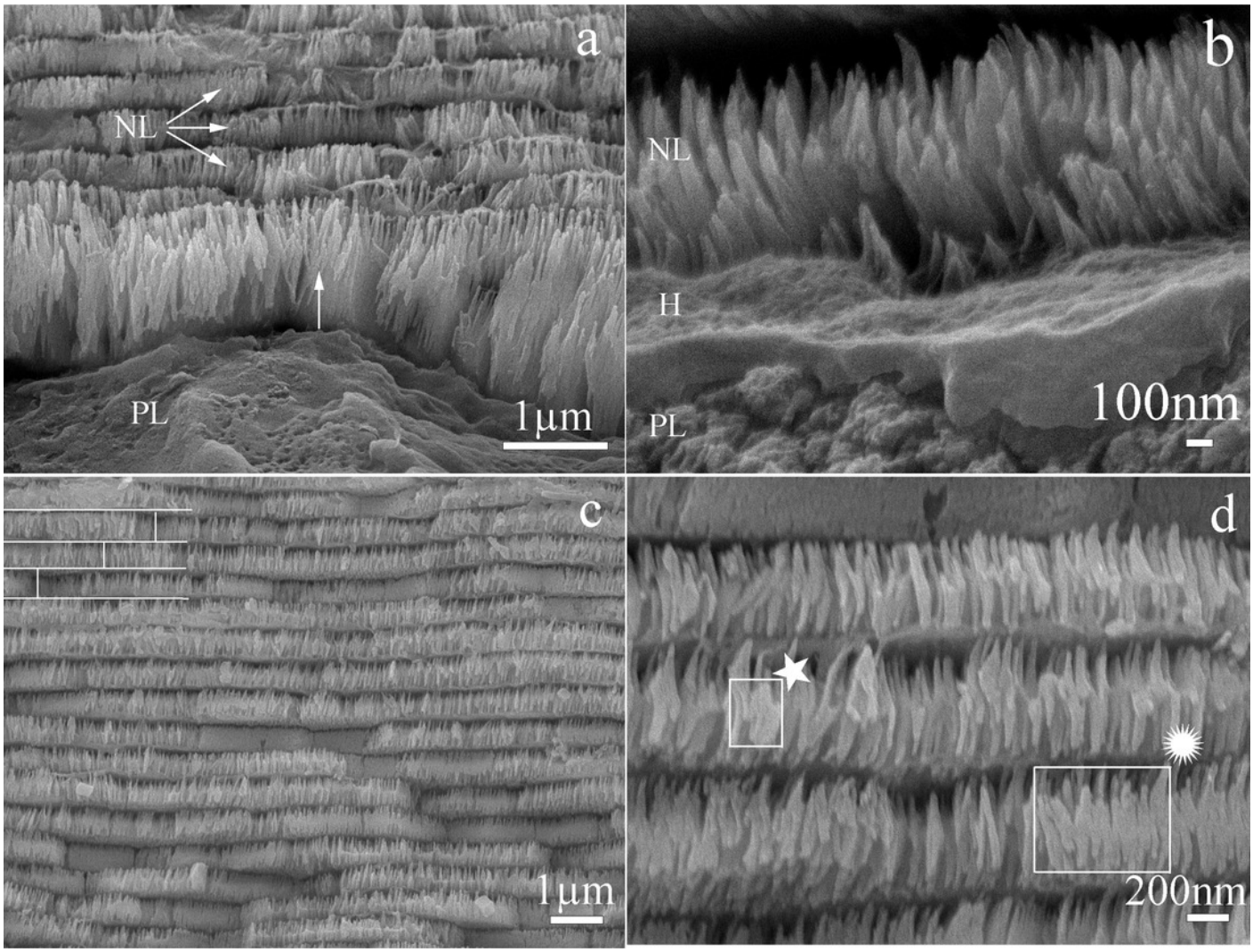
a
NL
PL
1μm
b
NL
H
PL
100nm
c
1μm
d
200nm

Figure 4

X-ray diffraction pattern of *P. colymbus* nacre powder.

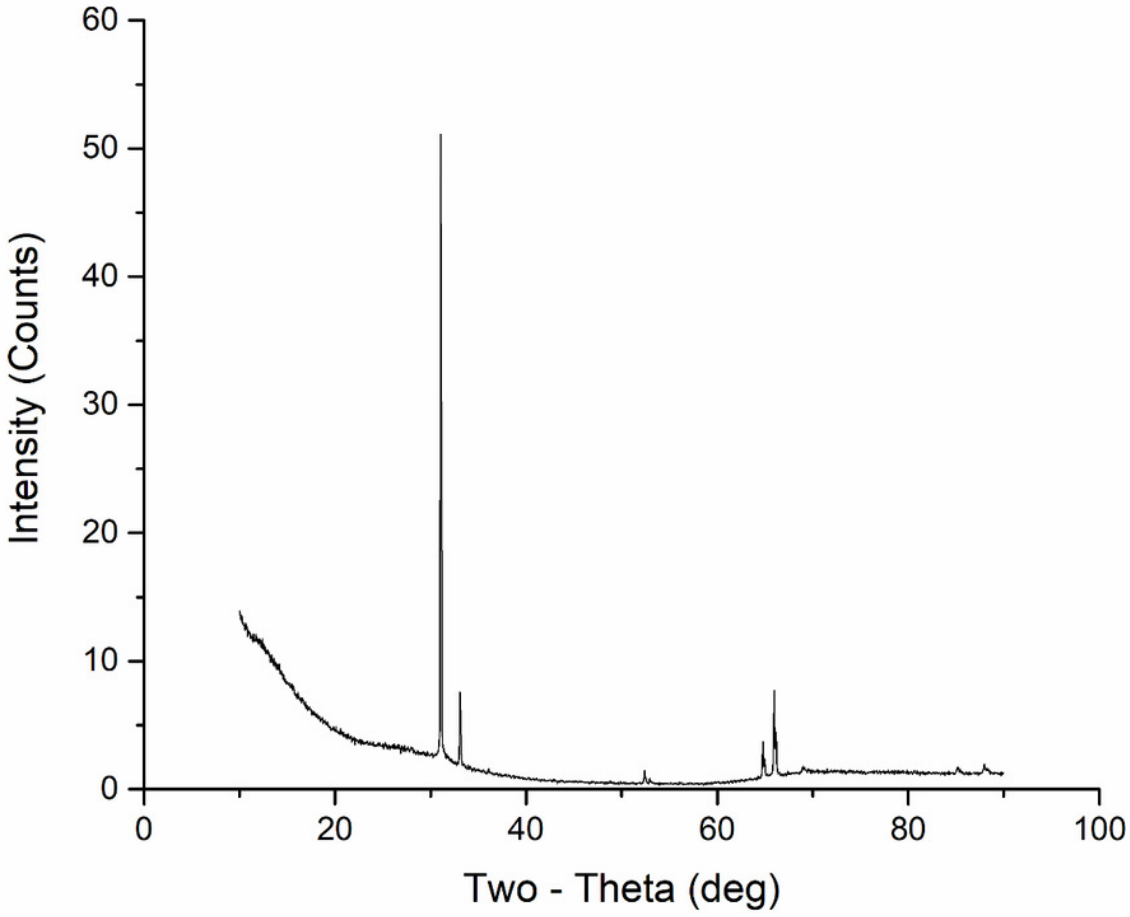

Figure 5

FTIR spectrum of *P. colymbus* nacre powder.

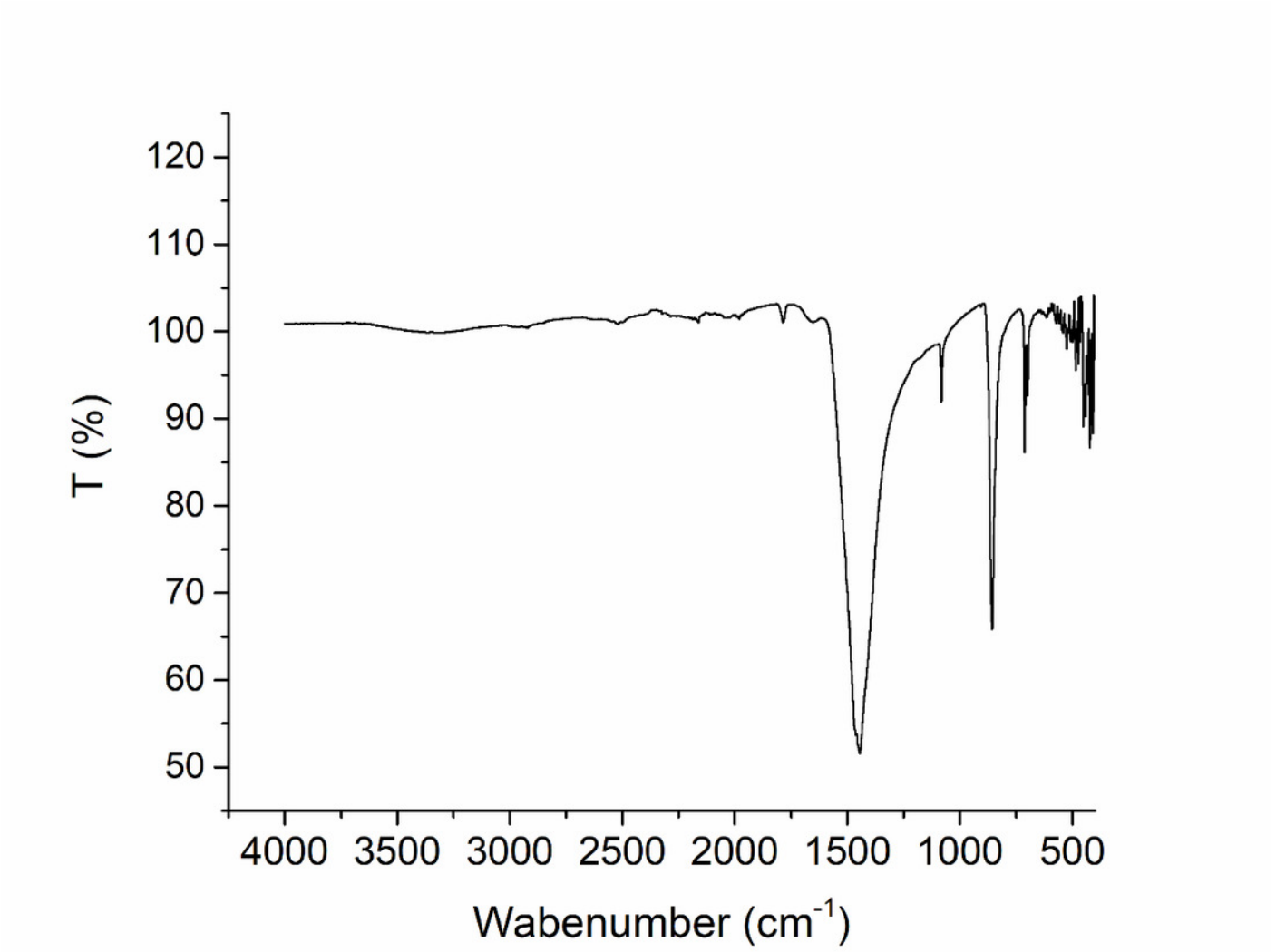

Figure 6

Raman spectrum of *P. colymbus* nacre powder.